Direct Observation of Adsorbed H_2-Framework Interactions in the Prussian Blue analogue $Mn^{II}_3[Co^{III}(CN)_6]_2$: The Relative Importance of Open Metal Sites and Van der Waals Interactions.

Karena W. Chapman,[,†] Peter J. Chupas,[*,†] Evan R. Maxey[‡] and James W. Richardson[‡]*

* chapmank@aps.anl.gov; chupas@aps.anl.gov

[†]Advanced Photon Source, Argonne National Laboratory.
[‡]Intense Pulsed Neutron Source, Argonne National Laboratory.

SUPPLEMENTAL INFORMATION

CONTENTS

Colour Figures

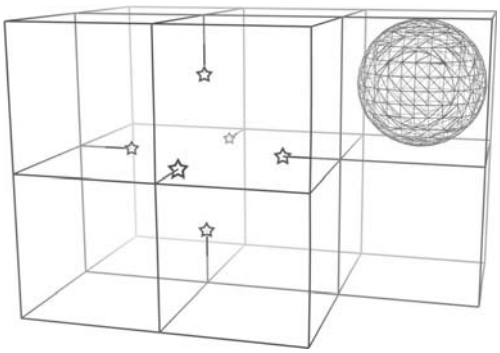

Fig. 1 Representation of the Prussian Blue network indicating the accessible Mn^{II} sites (star) surrounding a $Co(CN)_6^{3-}$ lattice vacancy. The lattice defines cavities of ~4 Å diameter connected by larger cavities associated with the aperiodic $Co(CN)_6^{3-}$ vacancies at one-third of the Co^{III} sites.

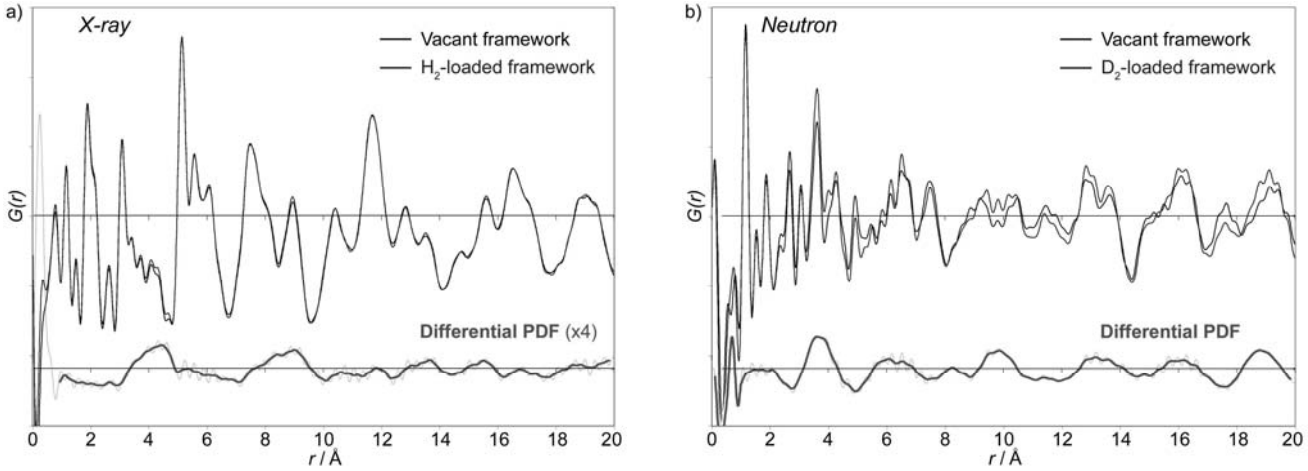

Fig. 2 The PDFs, *G(r)*, for the vacant and loaded framework and the corresponding differential PDFs from the X-ray (a) and neutron scattering data (b). The differentials, raw (dotted) and *r*-averaged over normalisation ripples (continuous), are shown.

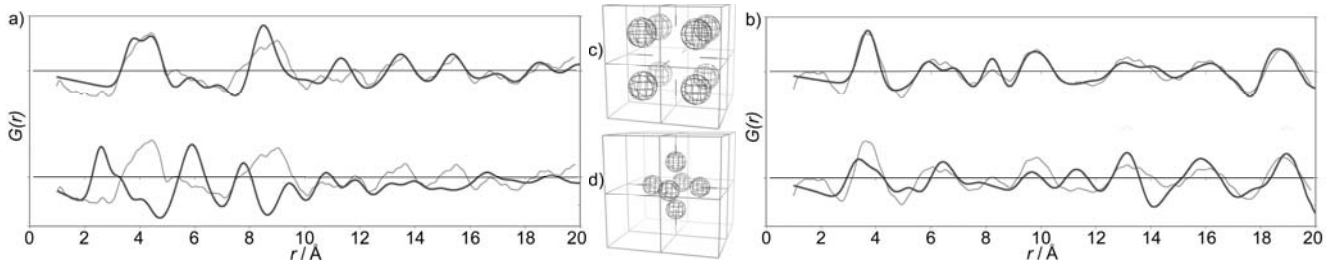

Fig. 3 Calculated X-ray (a) and neutron (b) differential PDFs for models consistent with van der Waals interactions (c, upper curves) and consistent with binding at the accessible Mn^{II} sites (d, lower curves). The experimental differentials (grey) are given for comparison.

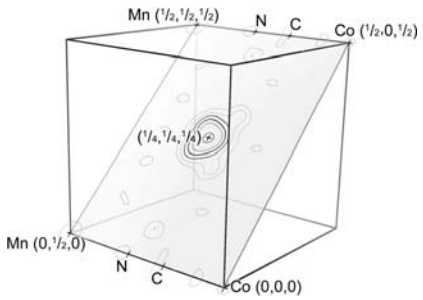

Fig. 4 Nuclear density Fourier difference map in the (011) plane from the Rietveld refinement of the D_2-loaded system at 77 K, modelling only framework atoms. Contours are drawn at 0.05 $\sigma Å^{-3}$ intervals. Levels below 0.15 (grey) are within the error in the data.

Sample Preparation

Crystalline samples of $Mn_3[Co(CN)_6]_2[H_2O]_6 . x\{H_2O\}$ ($x = 6 - 8$) was prepared by slow diffusion of aqueous solutions of the $MnCl_2$ (0.015 mol, 3.0 g) and $K_3Co(CN)_6$ (0.010 mol, 3.2 g) in water 400 mL at 60 °C. Very pale green crystals formed within 1-2 weeks and were filtered washed with water and ethanol and dried in air.

High Energy X-ray Scattering

A polyimide capillary-loaded sample of the hydrated phase, $Mn_3[Co(CN)_6]_2[H_2O]_6 . x\{H_2O\}$ was desolvated in-situ at 423 K under continuous helium (UHP) flow. The desolvated sample was cooled to 80 K* using an Oxford Cryosystems Cryostream 700 Plus and data were collected in both non-adsorbing helium and hydrogen (99.999%) gas atmospheres under continuous gas flow (ambient pressure) and at 25 psi overpressure. The high energy X-rays (90.48 keV, $\lambda = 0.1370$ Å) available at the 11-ID-B beamline at the Advanced Photon Source at Argonne National Laboratory, were used in combination with a General Electric Healthcare amorphous silicon detector to record diffraction patterns to high momentum transfer ($Q \sim 20.7$ Å^{-1}). Raw images were processed using Fit-2D[1] and the PDFs ($G(r) = 4\pi r[\rho(r)-\rho_o]$) were extracted within PDFgetX2 as described previously.[2, 3]

Time of Flight Neutron Powder Diffraction

A vanadium can-loaded sample (6 mL) of the hydrated phase was desolvated at 423 K under a dynamic vacuum. The sample temperature was controlled using a displex. Data were collected for the desolvated sample under vacuum and after loading with D_2 gas (1 atm, 77K) at 77 K and 30 K at the General Purpose Powder Diffractometer (GPPD) at the Intense Pulsed Neutron Source at Argonne National Laboratory. Raw data were scaled, corrected for detector efficiency, incident spectrum, sample holder and the PDFs were extracted within PDFgetN.[4]

---

* The minimum limit of the Oxford Cryosystems Cryostream 700 Plus is nominally 80 K. A temperature calibration suggested that the actual temperature may have been up to 15 K higher.

1. Hammersley, A. P., *ESRF Internal Report* **1997**, ESRF97HA02T.
2. Chupas, P. J.; Qiu, X.; Hanson, J. C.; Lee, P. L.; Grey, C. P.; Billinge, S. J. L., *J. Appl. Crystallogr.* **2003,** 36, 1342-1347.
3. Qiu, X.; Thompson, J. W.; Billinge, S. J. L., *J. Appl. Crystallogr.* **2004,** 37, 678.
4. Peterson, P. F.; Gutmann, M.; Proffen, T.; Billinge, S. J. L., *J. Appl. Crystallogr.* **2000,** 33, 1191-2.

X-ray & Neutron Pair Distribution Function Analysis

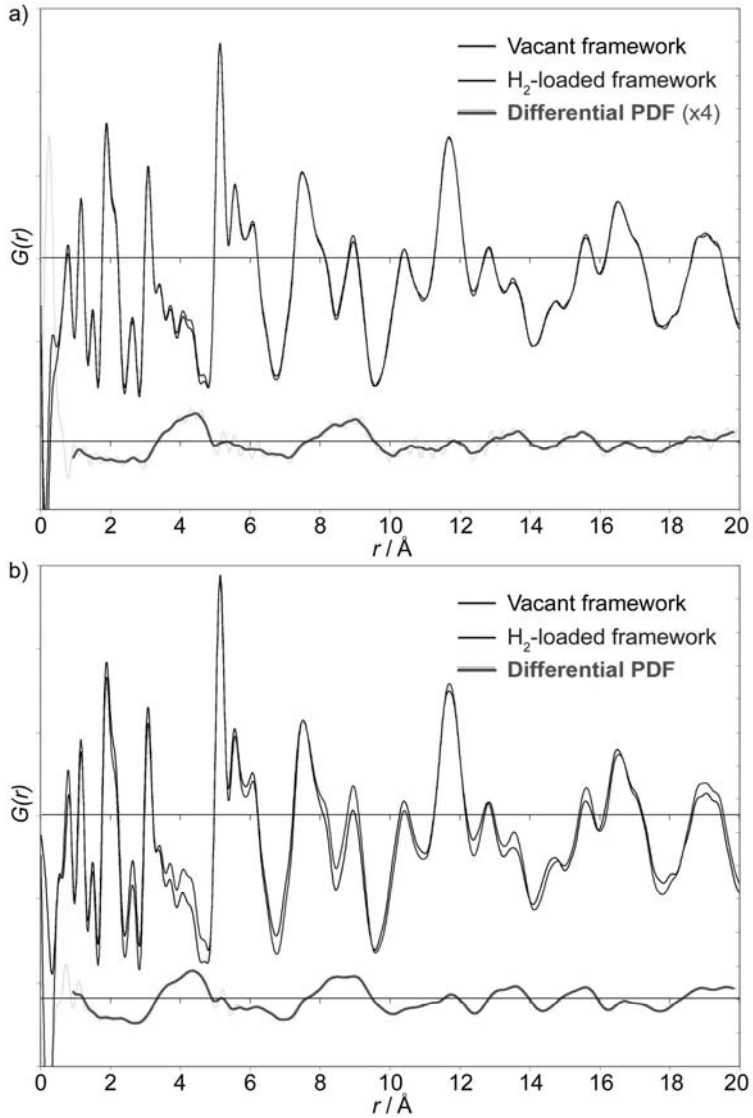

Figure S1. *The X-ray PDFs, G(r), for the vacant and H_2-loaded framework and the corresponding differential PDFs under gas flow (atmospheric pressure, a) and at 25 psi (b). The raw (dashed) and smoothed (continuous) differentials are shown.*

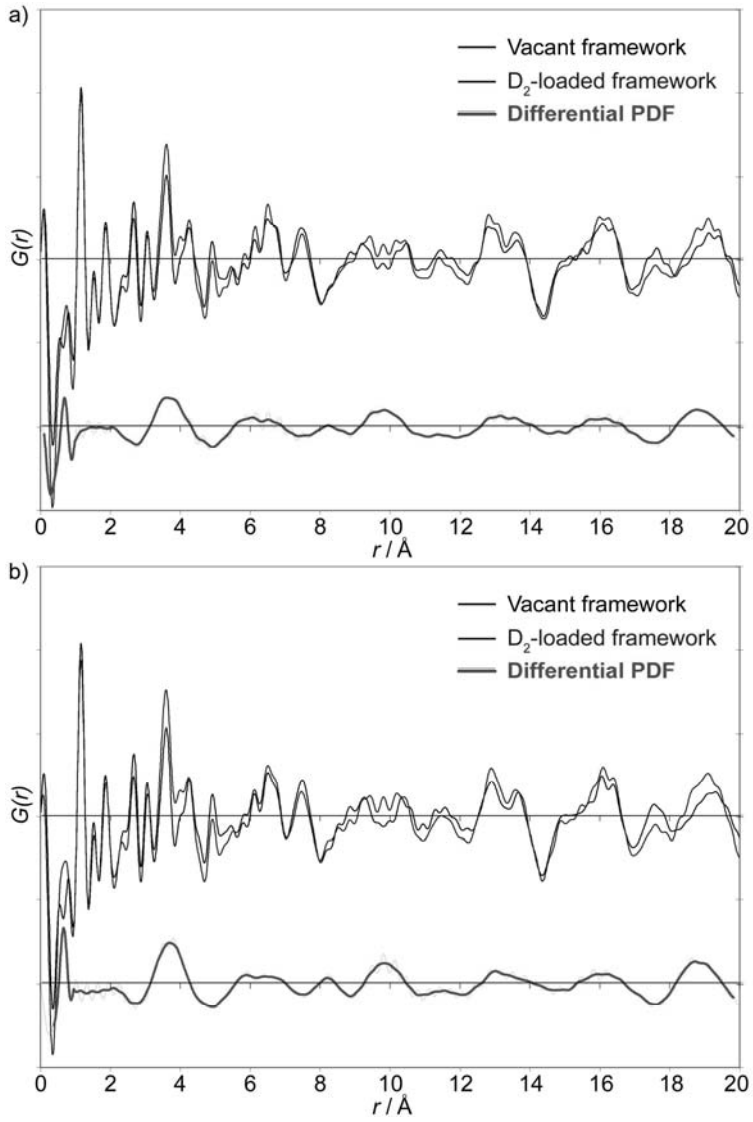

Figure S2. *The neutron PDFs, G(r), for the vacant and D_2-loaded framework and the corresponding differential PDFs 77 K (a) and 30 K (b). The raw (dashed) and smoothed (continuous) differentials are shown.*

Table S1. *Bond lengths extracted from the neutron PDFs for* ***$Mn_3[Co(CN)_6]_2$*** *and* ***$Mn_3[Co(CN)_6]_2 \bullet x\{D_2\}$*** *at 30 and 77 K.*

	$Mn_3[Co(CN)_6]_2$	$Mn_3[Co(CN)_6]_2$	$Mn_3[Co(CN)_6]_2\, x\{D_2\}$	$Mn_3[Co(CN)_6]_2\, x\{D_2\}$
T /K	30	77	77	30
$d_{D\text{-}D}$	-	-	0.6995(21)	0.635463(11)
$d_{C\text{-}N}$	1.13842(12)	1.13944(10)	1.14304(11)	1.13738(12)
$d_{Co\text{-}C}$	1.8897(31)	1.91403(10)	1.9667(19)	1.9075(15)
$d_{Mn\text{-}N}$	2.105(13)	2.08972(21)	2.1011(10)	2.0791(4)

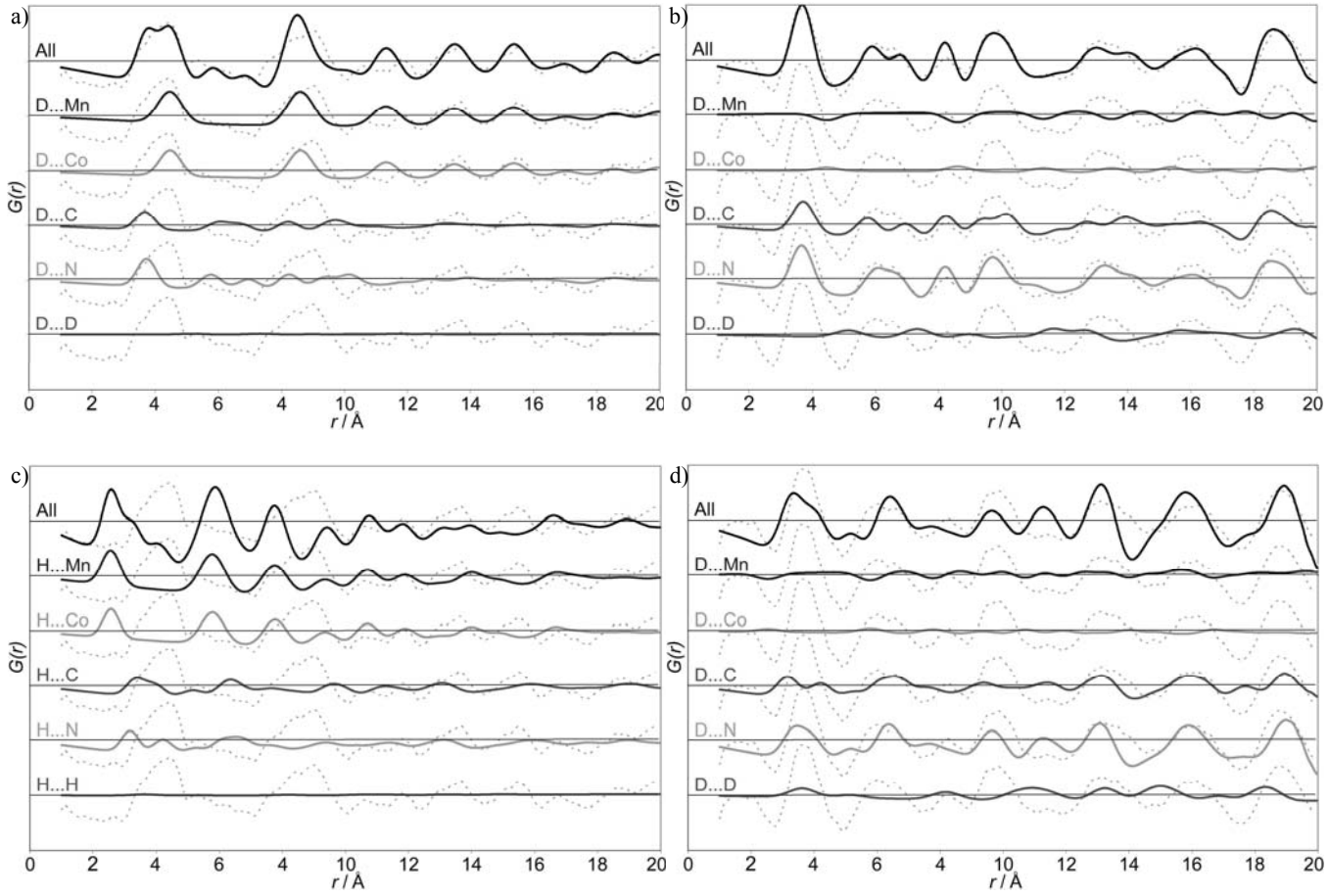

Figure S3. *Contributions to the X-ray (a,c) and neutron (b,d) PDFs, G(r), from guest-Mn, guest-Co, guest-C, guest-N and guest-guest atomic correlations calculated for models consistent with Van der Waals interactions (a,b) - H_2/D_2 at (¼, ¼, ¼) - and consistent with binding at the accessible coordination sites (c,d) - H_2/D_2 at (0, 0, x), x~0.25. The measured differentials at 80/77 K have been included for comparison (grey, dotted).*

Rietveld Analysis of Neutron Powder Diffraction

Rietveld refinements of the neutron powder diffraction data (5 detector banks) were performed within GSAS.

Table S2. *Rietveld analysis results for* ***$Mn_3[Co(CN)_6]_2$*** *and* ***$Mn_3[Co(CN)_6]_2 \bullet x\{D_2\}$*** *at 30 and 77 K.*

Compound		**$Mn_3[Co(CN)_6]_2$**	**$Mn_3[Co(CN)_6]_2$**	**$Mn_3[Co(CN)_6]_2\ x\{D_2\}$**	**$Mn_3[Co(CN)_6]_2\ x\{D_2\}$**
Formula		$C_{12}Co_2Mn_3N_{12}$	$C_{12}Co_2Mn_3N_{12}$	$C_{12}Co_2D_6Mn_3N_{12}$	$C_{12}Co_2D_6Mn_3N_{12}$
x		0	0	3	3
T /K		30	77	77	30
Space Group		$Fm\bar{3}m$	$Fm\bar{3}m$	$Fm\bar{3}m$	$Fm\bar{3}m$
a/Å		10.40005(8)	10.39633(8)	10.40011(8)	10.40294(10)
V/Å^3		1124.882(16)	1123.672(16)	1124.901(15)	1125.817(18)
Atomic position (*x*,*y*,*z*)	Co	(0,0,0)	(0,0,0)	(0,0,0)	(0,0,0)
	C	(0.17975(9),0,0)	(0.17984(8),0,0)	(0.17858(9),0,0)	(0.17981(10),0,0)
	N	(0.29180(7),0,0)	(0.29182(7),0,0)	(0.29058(8),0,0)	(0.29072(9),0,0)
	Mn	(0.5,0,0)	(0.5,0,0)	(0.5,0,0)	(0.5,0,0)
	D	-	-	(0.25,0.25,0.25)	(0.25,0.25,0.25)
Atomic displacement parameters / $\times 10^2$ Å^2	Co (U_{iso})	9.2(5)	9.7(5)	7.7(5)	7.4(6)
	C ($U_\perp$,$U_\parallel$)	4.83(6), 6.29(9)	4.94(5), 6.38(9)	4.94(5), 5.41(9)	4.82(6), 5.27(11)
	N ($U_\perp$,$U_\parallel$)	5.74(4), 4.13(5)	6.09(4), 4.09(5)	5.39(4), 4.93(6)	5.26(5), 4.55(7)
	Mn (U_{iso})	12.35(29)	12.55(27)	10.87(27)	11.25(35)
	D (U_{iso})	-	-	19.37(8)	13.75(7)
Bond lengths / Å	$d_{Co\text{-}C}$	1.8694(9)	1.8696(8)	1.8573(9)	1.8706(10)
	$d_{Mn\text{-}N}$	2.1653(8)	2.1643(7)	2.1780(8)	2.1771(10)
	$d_{C\text{-}N}$	1.1654(9)	1.1642(9)	1.1648(10)	1.1538(12)
d-spacing range / Å		6.7 - 0.88	6.7 - 0.88	6.7 - 0.88	6.7 - 0.88
Detector 2θ position/ ^{o}		145/125/107/90/30	145/125/107/90/30	145/125/107/90/30	145/125/107/90/30
χ^2		6.373	6.363	6.748	7.586
R_p /%		1.96	1.91	1.82	2.11
R_{wp} /%		2.55	2.50	2.45	2.89

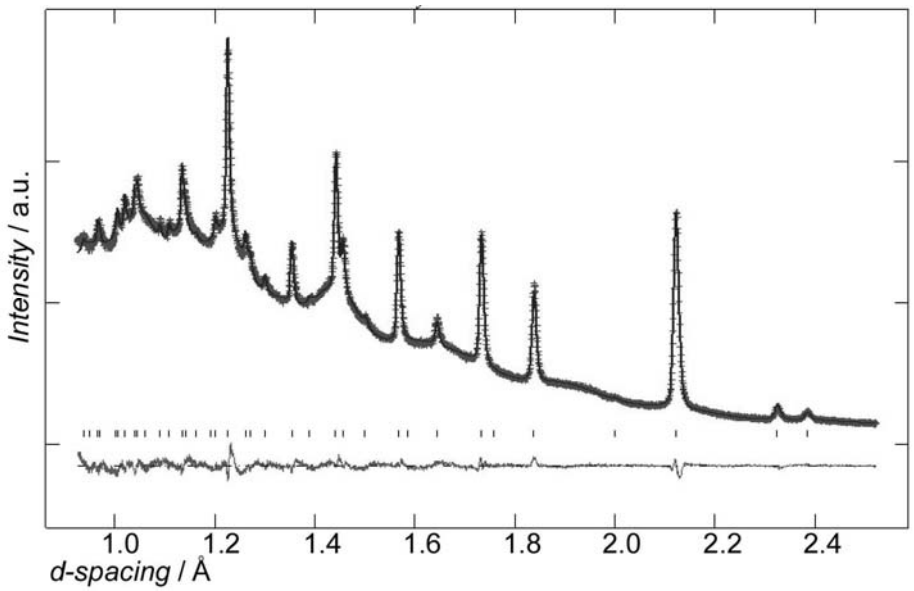

Figure S4. *A representative Rietveld refinement profile (histogram 2) for* $Mn_3[Co(CN)_6]_2$. *The data points (red crosses), model profile (blue line), reflection markers (vertical black lines) and residual (green lower line) are shown.*

Background Fitting

The background contained large diffuse contributions, most likely associated with short-range order of the aperiodic lattice vacancies and dynamic and static deviations of the structure from the average crystallographic positions. Different refinement strategies using a shifted Chebyshev polynomial (36 terms) and a diffuse scattering function background did not greatly affect the qualitative fit to the data or the refinement figures-of-merit. The reported refinements and difference maps are based on the diffuse scattering function background which minimised correlations between errors in the background, the model and Fourier difference maps.

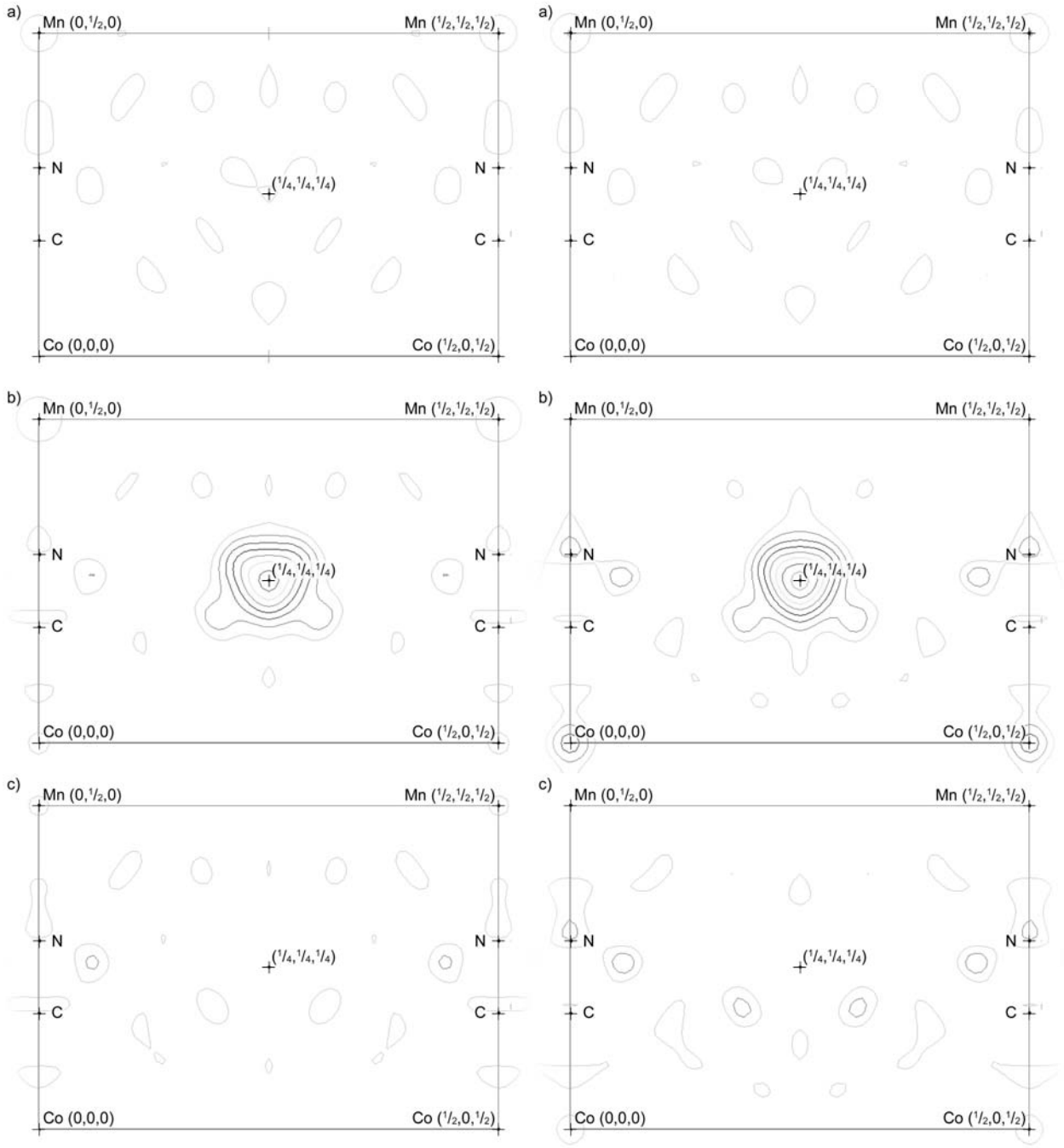

Figure S5. *Nuclear density Fourier difference maps from the Rietveld refinement of the structure of the nanoporous Prussian Blue analogue $Mn_3[Co(CN)_6]_2$ at 77 K and 30 K (left and right) for vacant (a) and D_2-loaded (unmodelled (b) and modelled (c)) frameworks. The plots show the (011) plane, centred at (¼, ¼, ¼). Contours are drawn at 0.05 $\sigma Å^{-3}$ intervals. Residual densities below 0.15 are not significant and are indicated in greyscale.*

Correlating Structure and Sorption Behaviour

Table S3. *Lattice parameters, pore dimensions and heats of sorption for* $M_3[Co(CN)_6]_2$.

Compound	M^{II} Ionic Radius[§] / pm	Lattice Parameter[†] a / Å	Pore Diameter[‡] / Å	$\Delta H_{Sorption}$[‖] / kJ mol^{-1}
$Mn_3[Co(CN)_6]_2$	97	10.40	4.10	5.3 - 5.9
$Fe_3[Co(CN)_6]_2$	92	10.25	4.00	6.3 - 6.6
$Co_3[Co(CN)_6]_2$	88	10.22	3.98	6.5 - 6.8
$Ni_3[Co(CN)_6]_2$	83	10.07	3.87	6.9 - 7.4
$Cu_3[Co(CN)_6]_2$	87	10.09	3.88	6.7 - 7.0
$Zn_3[Co(CN)_6]_2$	88	10.29	4.03	6.3 - 6.5

§ From Shannon, R., *Acta Crystallogr., Sect. A: Fundam. Crystallogr.* **1976,** 32, 751-767.
† For dehydrated phase at 100 K
‡ Estimated from lattice parameters using average Van der Waals radius for C and N (1.70 and 1.55 Å)
‖ From Kaye, S. S.; Long, J. R., *J. Am. Chem. Soc.* **2005,** 127, 6506-6507.

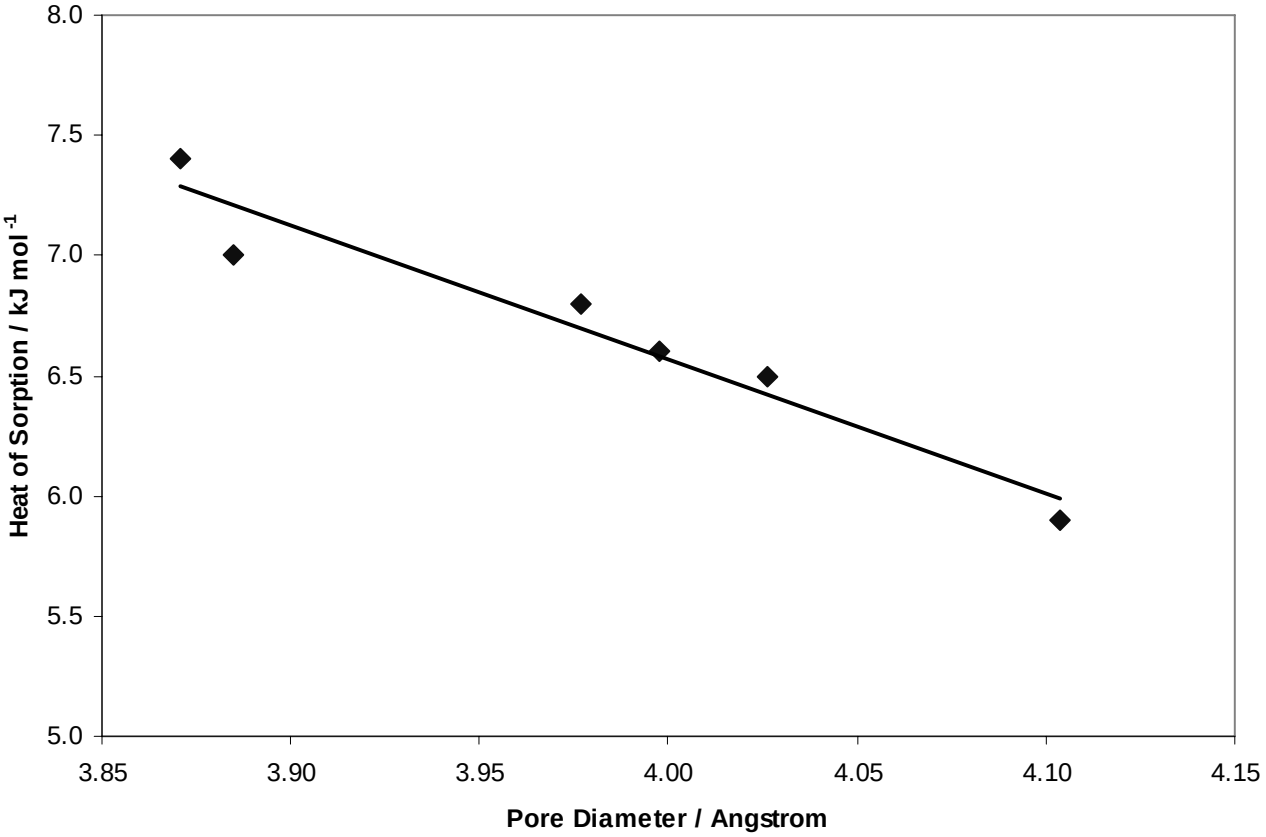

Figure S6. *The heats of sorption and pore diameters for* $M_3[Co(CN)_6]_2$.